AD-A124 942 IONOSPHERIC IRREGULARITIES AND THEIR POTENTIAL IMPACT 1/1
ON SYNTHETIC APERTURE RADARS(U) NAVAL RESEARCH LAB
WASHINGTON DC E P SZUSZCZEWICZ ET AL. 23 FEB 83
UNCLASSIFIED NRL-MR-4999 F/G 17/9 NL

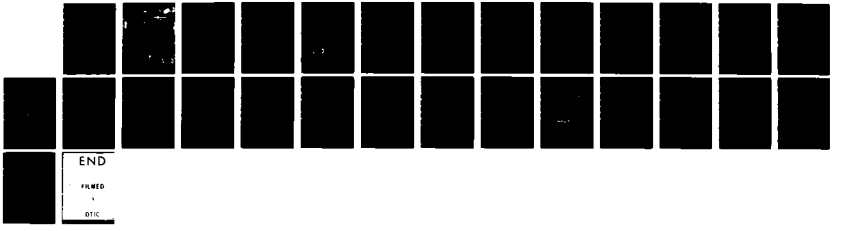

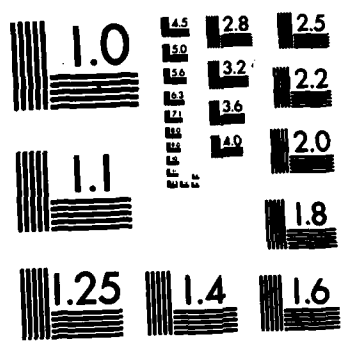

Ionospheric Irregularities and Equipotential Impact on Synthetic Aperture Radars

E. P. Szuszczewicz, M. Singh*, P. Rodriguez, and S. Mango†

Space Plasma Diagnostics Group
Space Science Division

**Sachs/Freeman Associates, Inc.*
Bowie, MD 20715

†*Space Sensing Applications Branch*
Aerospace Systems Division

February 23, 1983

This work was supported by the Office of Naval Research and Naval Electronic Systems Command

NAVAL RESEARCH LABORATORY
Washington, D.C.

SECURITY CLASSIFICATION OF THIS PAGE (When Data Entered)

REPORT DOCUMENTATION PAGE		READ INSTRUCTIONS BEFORE COMPLETING FORM
1. REPORT NUMBER NRL Memorandum Report 4999	2. GOVT ACCESSION NO. AD-A124 942	3. RECIPIENT'S CATALOG NUMBER
4. TITLE (and Subtitle) IONOSPHERIC IRREGULARITIES AND THEIR POTENTIAL IMPACT ON SYNTHETIC APERTURE RADARS		5. TYPE OF REPORT & PERIOD COVERED Interim report on a continuing NRL problem. 6. PERFORMING ORG. REPORT NUMBER
7. AUTHOR(s) E.P. Szuszczewicz, M. Singh*, P. Rodriguez and S. Mango		8. CONTRACT OR GRANT NUMBER(s)
9. PERFORMING ORGANIZATION NAME AND ADDRESS Naval Research Laboratory Washington, DC 20375		10. PROGRAM ELEMENT, PROJECT, TASK AREA & WORK UNIT NUMBERS 62712N; XF-12-141-350; 61153N; RR033-02-44; (Continues)
11. CONTROLLING OFFICE NAME AND ADDRESS Office of Naval Research Arlington, VA 22217 Naval Electronic Systems Command Washington, DC 20360		12. REPORT DATE February 23, 1983 13. NUMBER OF PAGES 26
14. MONITORING AGENCY NAME & ADDRESS(if different from Controlling Office)		15. SECURITY CLASS. (of this report) UNCLASSIFIED 15a. DECLASSIFICATION/DOWNGRADING SCHEDULE

16. DISTRIBUTION STATEMENT (of this Report)

Approved for public release; distribution unlimited.

17. DISTRIBUTION STATEMENT (of the abstract entered in Block 20, if different from Report)

18. SUPPLEMENTARY NOTES

*Present address: Sachs/Freeman Associates, Inc., Bowie, MD 20715

This work was supported by the Office of Naval Research and Naval Electronic Systems Command

19. KEY WORDS (Continue on reverse side if necessary and identify by block number)

Synthetic aperture radar (SAR)
Ionospheric irregularities
Aurora
Spread-F
Scintillations

20. ABSTRACT (Continue on reverse side if necessary and identify by block number)

Accumulating data are making it increasingly evident that major plasma irregularities populate substantial portions of the ionosphere. In contrast with these findings, satellite-borne synthetic aperture radar (SAR) systems tacitly assume that the ionosphere is uniformly layered and unchanging under the orbiting SAR. Analysis of plasma irregularity structures measured directly on the S3-4 satellite shows that this assumption is readily violated near the nighttime equator during the occurrence of spread-F and at all high-latitudes on a nearly 24 hour basis. The irregularities can be very intense,

(Continues)

DD FORM 1 JAN 73 1473 EDITION OF 1 NOV 65 IS OBSOLETE
S/N 0102-014-6601

SECURITY CLASSIFICATION OF THIS PAGE (When Data Entered)

10. Program Element, Project, Task Area and Work Unit Numbers (Continued)

41-0949-0-3; 41-0999-A-2

20. Abstract (Continued)

covering scale sizes from meters to hundreds of kilometers. Associated along-track phase path calculations point to a potentially serious problem in SAR imaging integrity in restricted ionospheric space-time domains.

CONTENTS

IONOSPHERIC IRREGULARITIES AND THEIR POTENTIAL IMPACT ON SYNTHETIC APERTURE RADARS

I. INTRODUCTION

Accumulating information is making it increasingly evident that major plasma irregularities populate a substantial portion of the Earth's F-region ionosphere. In fact, the occurrence frequencies and geographical distributions of such ionospheric structures are of such a magnitude as to suggest that smooth, slowly-varying ionospheric models should be used with caution in calculations intended to define the propagation characteristics of transionospheric electromagnetic waves.

In considering the imaging capability of satellite-borne synthetic aperture radars (SAR), it is generally assumed that the ionosphere is uniform and unchanging under the orbiting SAR...an assumption relevant to imaging integrity requiring a constant two-way phase path length from the satellite-to-ground over the full aperture width. Analysis of the S3-4 satellite data [Szuszczewicz et al., 1982a; Szuszczewicz et al., 1982b] suggests that this assumption can be substantially violated (e.g. phase path variations can be several times the wavelength of the probing radar) over specific segments of a given orbit.

Figure 1 presents a phenomenological perspective of various geoplasma domains covered in the S3-4 investigation. The schematic presentation is in the noon-midnight meridian, with the midnight equator at the very left of the figure, the north polar cap in the center, and the noontime equator to the right. The ionospheric plasma "biteouts" illustrated at nighttime equatorial latitudes represent one of the most dramatic features of ionospheric structure studied in the S3-4 effort. These "biteouts" are naturally occurring ionospheric holes which can have widths ranging from fractions of a meter to tens of kilometers [McClure and Hanson, 1973; McClure and Hanson, 1977; Szuszczewicz, 1977; Szuszczewicz et al., 1981]. There can be major changes in ion chemistry which take place across the boundaries of the holes...changes which now appear to be trendable and coupled to the mechanisms which generate the holes themselves [Szuszczewicz et al., 1980; Narcisi and Szuszczewicz, 1981; Keskinen et al., 1981] and cascade the irregularity distributions from tens of kilometers to fractions of a meter [Kelley et al., 1982]. These irregularities, generally identified with the disturbed ionospheric state called equatorial spread-F, are responsible for nighttime equatorial scintillations known to seriously limit the reliability of communication satellites.

Manuscript approved December 9, 1982.

Outside the nighttime equatorial domain, the regions of primary interest in the S3-4 study of F-region irregularities involve the main trough, auroral oval, and the ionospheric domains encompassing the ring current, polar wind and the cusp. In this high-latitude F-region, large-scale density irregularities are routinely detected [Rodriguez et al., 1981]. The absolute density variations can be as large as an order of magnitude and in the case of a quiet diffuse aurora, the irregularities appear to be consistent with the sheet-like structures that have been postulated to explain high-latitude scintillation enhancements [Fremouw et al., 1977; Rino et al., 1978]. In general, energetic particle precipitation patterns, plasma instability processes and cross polar cap convection all play important roles in determining irregularity scale size distributions and relative intensities in the high-latitude regime.

In contrast to the generally irregular ionospheric state at the nighttime equator and polar regions, the mid-latitude and dayside equatorial F-regions are generally very regular in structure and consequently of significantly less impact on transionospheric propagation characteristics.

To help develop a quantitative measure of potential ionospheric effects on SAR operations, Figure 2 presents a schematic of a typical satellite SAR system along with the characteristics of the Seasat SAR. The general SAR system under consideration is a satellite-borne, side-looking imaging radar which transmits a series of short coherent pulses to some target within the beam's footprint on the Earth. Any particular target is illuminated by the radar beam for a finite time T equal to L/v_{sc}, where L is the along-track dimension of the footprint and v_{sc} is the spacecraft velocity. During the time T, the slant-range component of the spacecraft's velocity relative to the target is constantly changing, yielding a time-dependent Doppler shift in the frequency of the return pulses. The Doppler phase history can then be used to distinguish between any number of targets within the same footprint. Thus, the radar's illumination of any target is equivalent to that from a synthetic aperture of length $L=v_{sc}T$.

The processing of SAR data may be optical or digital, and in either case involves a complicated, time-consuming procedure which will not be described here. [see e.g., Tomiyasu, 1978; Harger, 1970; Wu, 1980]. The singularly important point, however, is that the basic premise for successful processing of satellite SAR data is that the phase and amplitude of the radar is known or can be modelled throughout the end-to-end system so that the required coherency of the SAR radiation can be preserved in the processing. This includes any phase/amplitude variations introduced by the SAR transmitter, receiver, or antenna system as well as by the two-way traversal of the SAR beam through the Earth's atmosphere and ionosphere. The tacit

assumption to date has been that the ionosphere and troposphere introduce only a negligible or, at worst, a uniform phase/amplitude variation across the SAR beam and from beam-to-beam as the vehicle moves along track. Basically this assumes there are no differential phase/amplitude effects in time or space over the SAR data set.

Ionospheric effects which attenuate the amplitude of the SAR signals are not as crucial to the SAR processing in the sense that the all important phase coherency of the SAR signals is not altered. In many respects, ionospheric phenomena that affect the phase of the SAR signals are much more significant and insidious. Even if one assumes a well-designed overall SAR system (including processor), differential phase effects in both the spatial and temporal domains may lead to coherency break-up which may be extremely difficult, if not practically impossible, to compensate for. This means that the information content and interpretability of final SAR images may be more tolerant to amplitude effects than to phase effects. The most important point for all SAR processing is that any and all significant phase variations due to all causes must be known or must be modelled accurately in order to produce good SAR imagery. This statement can be reduced to a measureable figure of merit by requiring that the two-way phase path for a given object be unchanged over the entire synthetic aperture width. Thus, SAR imaging integrity demands

$$\Delta P = 2\left\{\int_{R_1} \eta ds - \int_{R_2} \eta d\varepsilon\right\} << \lambda_o/2 \qquad (1)$$

where η is the ionospheric index of refraction

$$\eta = 1 - k_1 \frac{N_e}{f^2} \pm k_2 \frac{N_e B \cos\theta}{f^3} - \frac{k_3 N_e^2 + k_4 N_e B^2 (1 - \frac{1}{2}\sin^2\theta)}{f^4} + \ldots \qquad (2)$$

$$\simeq 1 - k_1 (N_e/f^2). \qquad (3)$$

with

$N_e \equiv$ position-dependent ionospheric density,

$B \equiv$ strength of the Earth's magnetic field,

$\theta \equiv$ angle between SAR wave normal and the Earth's B-field.

$f \equiv$ SAR frequency

$\lambda_o \equiv$ SAR wavelength (23.5cm for Seasat), and

$R_i \equiv$ slant range at the i_{th} position within a given aperture width.

That condition (1) can be substantially violated will be demonstrated in subsequent sections, and initial estimates for a global perspective on ionospheric-related SAR effects will be presented.

II. PHASE PATH VARIATIONS

A. Estimates from Rocket-Borne Ionospheric Data

To establish an initial estimate of phase path variations due to ionospheric effects consider the ionospheric profile in Figure 3. A rocket payload carrying "in situ" plasma diagnostic devices was launched into the nighttime equatorial ionosphere under conditions of well-developed spread-F and revealed a vertical plasma distribution which differed significantly from that which a zero-order laminar ionospheric model would predict.

The results in Figure 3 show the F-peak at 375 km, with a maximum density of 1.3 (10^6) cm^{-3} ($\pm$ 10%). The probe measurements also revealed a number of major depletions ("biteouts") distributed throughout the F-region with each of the depletions having been shown to have its own set of smaller-scale irregularities [Keskinen et al., 1981].

To illustrate the potential impact of such ionospheric structure on the SAR condition Equ (1), a two-way phase path calculation was done assuming a Seasat SAR operating at 800 km with a 1.2 GHz frequency. If the SAR "saw" the Figure 3 zero-order profile at one time within a given synthetic aperture ($\sim$16 km) and the actual spread-F profile at another time (and position) within the same aperture, the phase path difference would not be $\Delta P << \lambda_o/2$, but in fact

$$\Delta P = 9 \text{ meter} \simeq 36\lambda_o .$$

If the assumed scenario actually occurred, the SAR condition (1) would be violated.

While the data in Figure 3 reflect conditions which do exist at the nighttime equator, the ΔP calculation employed an artificial boxcar profile along the horizontal aperture. To more fully explore the effects along the satellite track and the significance of irregularity scale size distributions relative to a typical aperture length, additional analysis focused on the "in situ" ionospheric plasma density data collected in the S3-4 satellite mission [Szuszczewicz et al., 1982a,b]. This focus was established on the basis of four points: (1) Irregularity measurements covered scales from several meters to hundreds of kilometers, (2) Ionospheric domains included day/night and equatorial-, mid- and high-latitudes, (3) The altitude was near the F-region peak density, and (4) The Seasat and S3-4 mission lifetimes had significant portions of overlap, leaving open the possibility for coincident and correlated observations as a follow-up to this investigation.

B. Estimates from S3-4 Satellite Data

The S3-4 satellite was launched into polar orbit in March 1978 and operated successfully for a planned 6 month mission which closed in September of the same year. The polar F-region orbit (appr. 165 km x 260 km) made possible a global study of F-region ionospheric electron densities N_e, temperature T_e, irregularity structures δN_e, and associated power spectral distributions $P_n(k)$. The data provided a fundamental base upon which to catalogue similarities and differences between polar and equatorial irregularities and ultimately sort out causal mechanisms which couple plasma instabilities, ionospheric irregularities, and associated effects on communication and surveillance systems. From a data base which included over 600 orbits during the March-September 1978 period a set of highly disturbed ionospheric profiles was selected as an initial test bed for SAR considerations. These profiles focussed on two major domains: (i) the nighttime equatorial regimes which analyses suggest presents a significant source of potential SAR difficulty in terms of irregularity intensities, and (ii) the high-latitude regime which is disturbed nearly on a 24 hour basis. The S3-4 data also suggested that other ionospheric domains (e.g. nighttime/daytime midlatitudes and dayside equatorial) are substantially less irregular and consequently less threatening to SAR imaging capabilities.

Equatorial regime. Figure 4 presents a 260 sec along-track segment ($\tilde{\sim}$1900 km) of "in situ" S3-4 density measurements in the nighttime equatorial F-region. The central panel is a plot of absolute density N_e showing major depletions in the 1-to-100's of kilometer domain.

Detrended formats of the same profile are presented in the upper panel in terms of relative density fluctuations $\Delta N_e/N_e$ and in the lower panel in terms of absolute RMS fluctuations $(\Delta N_e)_{RMS}$. The data is very typical of a well-developed spread-F ionosphere in that peak densities are near 10^6 cm^{-3}, depletions can be greater than an order of magnitude, and the scale size distribution covers a very broad spectrum.

To determine the ΔP figure of merit relevant to SAR operations, we have adopted the vertical Chapman profile shown in Figure 5 and have assumed the satellite profile of Figure 4 to map 50 km in vertical extent and to be centered at the F-peak. In terms of potential phase path effects, this defines a severe, but not necessarily worst-case situation, for we assume the entire top and bottomside F-region is quiescent (unlike Figure 3).

Proceeding with the above F-region plasma distribution functions, the associated two-way phase path fluctuations (over a two-way rectilinear length of 1600 km) for a Seasat-type SAR are presented in Figure 6. The abscissa corresponds

identically with that in Figure 4 while the right-hand ordinate shows that over the data segment in question the phase path variations are bounded within a maximum excursion of 3.36 meters (16.16-12.80 m), that is,

$$\Delta P \text{ (max)} = 3.36 \text{ meters} = 14.3\lambda_o.$$

Since the correlation lengths in Figure 6 are generally too large for direct SAR-aperture comparisons, smaller segments of the data are expanded and presented in Figures 7 and 8, 21.32 sec (160 km) segments A, B and C and 2.12 sec (16 km) segments a, b and c, respectively. The 160 km samples approximate 10 synthetic aperture lengths for a Seasat system, while the 16 km samples represent a single aperture length. The data show the broad range of phase path fluctuations and their intrinsic nondeterministic nature. Within the data samples are relatively smooth low frequency oscillations (Figure 8, panel "a") with along-track gradients in phase path variations of the order $\Delta P=7\lambda_o$ per kilometer. Higher frequency oscillations are also evident (Figure 8, panel "b") with much steeper gradients in phase path variations (e.g. $\Delta P=34\lambda_o$ per kilometer).

High Latitude Regime. Next to the nighttime equatorial domain, the high-latitude ionosphere appears to present the most serious natural threat to the imaging capabilities of a satellite-borne SAR. From a phenomenological perspective Figure 9 illustrates a source-term map of high-latitude ionospheric irregularities across the polar cap. Discrete auroral arcs and cusp region irregularities can be characterized as relatively intense structures ($\delta N_e/N_e \gtrsim 1$) of narrow horizontal extent (< 10's of kilometers), whereas diffuse aurora can be thought of as more smoothly varying structures extending over broader regions of space (e.g. 100 km). The map in Figure 9 can be viewed as a general pictorial display of high latitude morphology but caution is advised in any specific application because marked space and time variations in ionospheric-magnetospheric coupling processes can dramatically alter the configuration.

Figure 10 presents a polar-cap segment of S3-4 data. The presentation is identical to that used previously in Figure 4 with upper, middle, and lower traces depicting the fundamental density profile in terms of relative fluctuations, absolute in-track electron densities, and RMS fluctuations, respectively.

Figure 11 is a 150 second ($\gtrsim$ 1100 km) expanded view of the absolute density profile segment centered near the 2211 UT period in Figure 10, while the four panels in Figure 12 present 20 second ($\gtrsim$ 160 km) breakouts of regions A, B, C, and D. The segments of 160 km are approximately equal to 10 synthetic aperture lengths.

To determine the ΔP figure of merit relevant to SAR operations, we assumed a value of 10^{17} electrons-cm^{-2} as a nominal high-latitude TEC and then allowed associated percent fluctuations to vary in direct correlation with the in-track density profile. This is tantamount to assuming that all ionospheric variations are flux tube alighned at high-latitudes and shape-preserving along the field. With this model, phase path variations were calculated for the 2-second (approximately 1 synthetic aperture) segments a, b, c, and d in Figure 12. The variations are seen to cover the relatively smooth, somewhat innocuous behavior in panel "a" with $\Delta P(max) = 2.5$ meters $\approx 10\lambda_o$, to the rapidly-varying, highly-structured behavior with along-track gradients in ΔP as large as $180\lambda_o$ per km for a Seasat-type SAR system. Comparison of the results in Figure 12, with those in Figure 8, shows the high-latitude regime as a more highly structured regime when measured in terms of gradients in ΔP.

III. COMMENTS AND CONCLUSIONS

Analysis of "in situ" S3-4 satellite data on ionospheric irregularities at F-region altitudes has shown that ionospheric structures encompass an extremely broad range of scale sizes, ranging from tens of kilometers to meters. The overall results show large populations of intense irregularities which are comparable to and smaller than nominal synthetic aperture lengths (approximately 16 km).

Conclusions point to a fundamental problem in SAR imaging integrity in that the tacit assumption that "ionospheric effects can be ignored" appears in violation of documented irregularity distributions.

Accumulated data show that the nighttime equatorial domain ($\approx$ 7 PM to 2 AM LT (with seasonal, solar-cycle and day-to-day variations superimposed), $|MLAT| \lesssim 20^o$) and the high-latitude regimes ($|MLAT| \gtrsim 55^o$ on a nearly 24 hour basis) appear to present the most serious natural ionospheric threat to satellite-borne SAR imaging capabilities. Calculated phase path variations include both high and low-frequencies with $\Delta P = 34\lambda_o$ and $\Delta P = 180\lambda_o$ representative of the highest level gradients in phase path variations per km (along-track) at nighttime-equatorial and high-latitudinal domains, respectively. The dayside hemisphere at equatorial and mid-latitudes ($|MLAT| \lesssim 55^o$) appears to present very little threat; as does the nightside midlatitude domain ($20^o \lesssim |MLAT| \lesssim 55^o$).

The results are based on actual "in situ" satellite measurements of irregularity distributions in and around the F-region peak complemented by assumed vertical ionospheric profiles considered nominal for local phenomenology. In this sense the ΔP calculations are model-dependent. In

contrast, the morphology of irregularity distributions and discussions relevant to potential SAR effects are model-independent and stand on their own merit.

By way of additional comment we note that a casual reader may suggest that there exists an apparent paradox since there is a history of successful imagery from SAR systems. For example, aircraft systems have long been successful...but these sensors, of course, were not high enough in altitude to be affected by the ionosphere. In addition, there exists excellent L-band SAR imagery from Seasat orbiting at an altitude of 800 km and more recently from SIR-A flown on the Space Shuttle at an altitude near 250 km. In the case of Seasat only the "quiet" mid-northern-latitudes were imaged with a few excursions into MLAT > 55^{o} domains. Our results would have predicted undisturbed imaging at midlatitudes. Several of the higher-latitudinal Seasat passes were "not processible"...a result which we intend to investigate for correlation with ionospheric irregularities. Some initial work has been done along these lines by the Defense Nuclear Agency (H.C. Fitz, private communication) showing image degradation at high-latitudes that could be attributed to ionospheric disturbances. While Seasat had no equatorial coverage, SIR-A did cover the nighttime equatorial domain for several days during its Shuttle mission. The occurrence statistics of spread-F during that mission have not yet been established nor have the causal relationships for a number of unprocessible SIR-A imaging segments.

Finally we note that the $\Delta P << \lambda_o/2$ condition becomes less stringent with increasing SAR frequency...a result that becomes clear in rewriting Equ. (1) as

$$4c^{-1}k_1 \left\{ \int_j^i [N_e(1) - N_e(2)]\, ds \right\} << f. \qquad (4)$$

The above inequality is a straightforward manipulation of condition (1) with $f=c/\lambda_o$. Had our "test" frequency been 12 GHz instead of the Seasat frequency of 1.2 GHz all ΔP results would have been reduced by a corresponding order of magnitude. The steepest reported gradient for a 12 GHz system would have been $\Delta P=18\lambda_o$. For a 120 GHz system that same result would have become $\Delta P=1.8\lambda_o$... and so on. Clearly some options could be made available with attendant trade-off studies in order. Additional studies should include polarization effects and considerations related to cross-track distortions in SAR imaging. In this paper, we addressed only primary phase effects in the along-track (azimuth) direction.

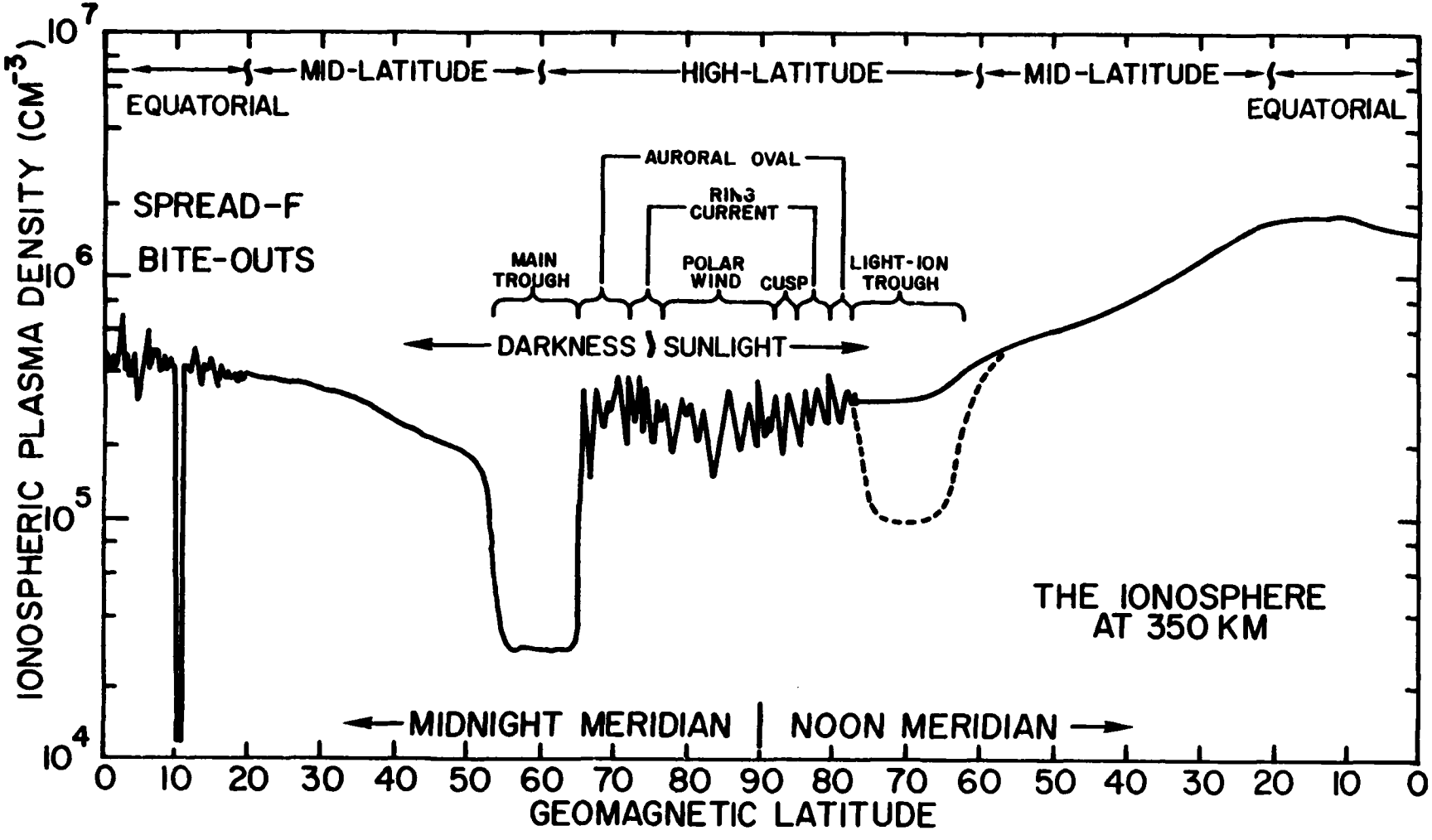

Figure 1. Phenomenological perspective of various geoplasma domains in the S3-4 investigation. [From Szuszczewicz et al., 1982a]

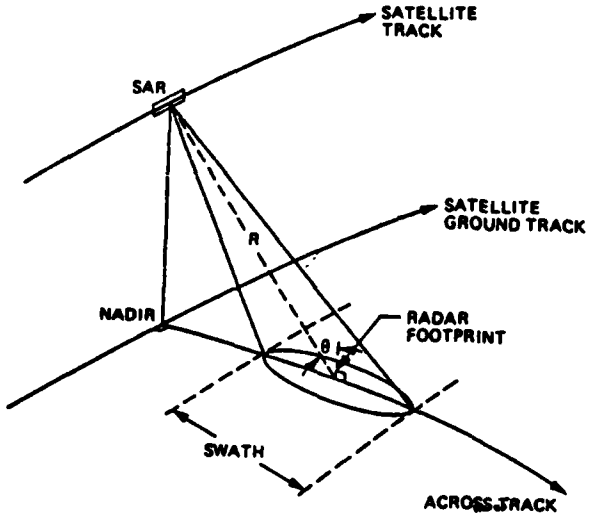

SATELLITE ALTITUDE, INCLINATION	800 KM, 108°
RADAR FREQUENCY, WAVELENGTH	1.275 GHz, 23.5 CM
AZIMUTH BEAMWIDTH, APERTURE LENGTH	~1.1°, ~16 KM
SWATH WIDTH	100 KM
THEORETICAL RESOLUTION ON THE SURFACE	25 M X 25 M
ANTENNA DIMENSIONS, LOOK ANGLE	10.74 M X 2.16 M, 20° FROM VERTICAL
INCIDENCE ANGLE ON THE SURFACE	23° ± 3° ACROSS THE SWATH
TRANSMITTED PULSE LENGTH	33.4 μS
PULSE REPETITION FREQUENCY (PRF)	1463 TO 1640 PPS
SYSTEM BANDWIDTH	19 MHz
TIME-BANDWIDTH PRODUCT	634

Figure 2. SAR imaging geometry and Seasat characteristics. (Adapted from "Seasat Views Oceans and Sea Ice with Synthetic-Aperture Radar", by L. Fu and B. Holt, JPL Publication 81-120, (February 15, 1982))

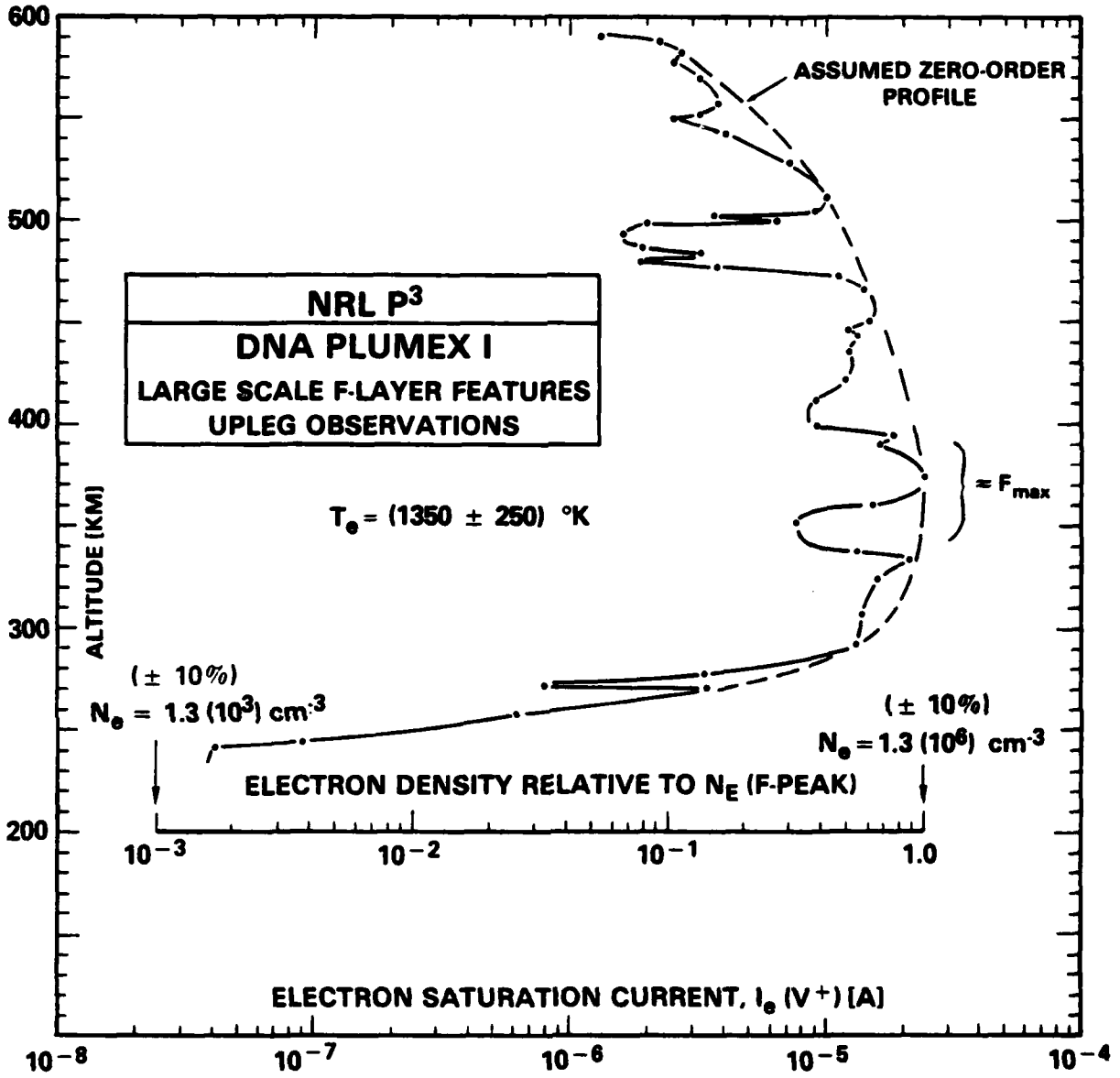

Figure 3. Vertical profile of ionospheric F-region density as measured directly by rocket-borne instrumentation during the occurrence of equatorial spread-F.

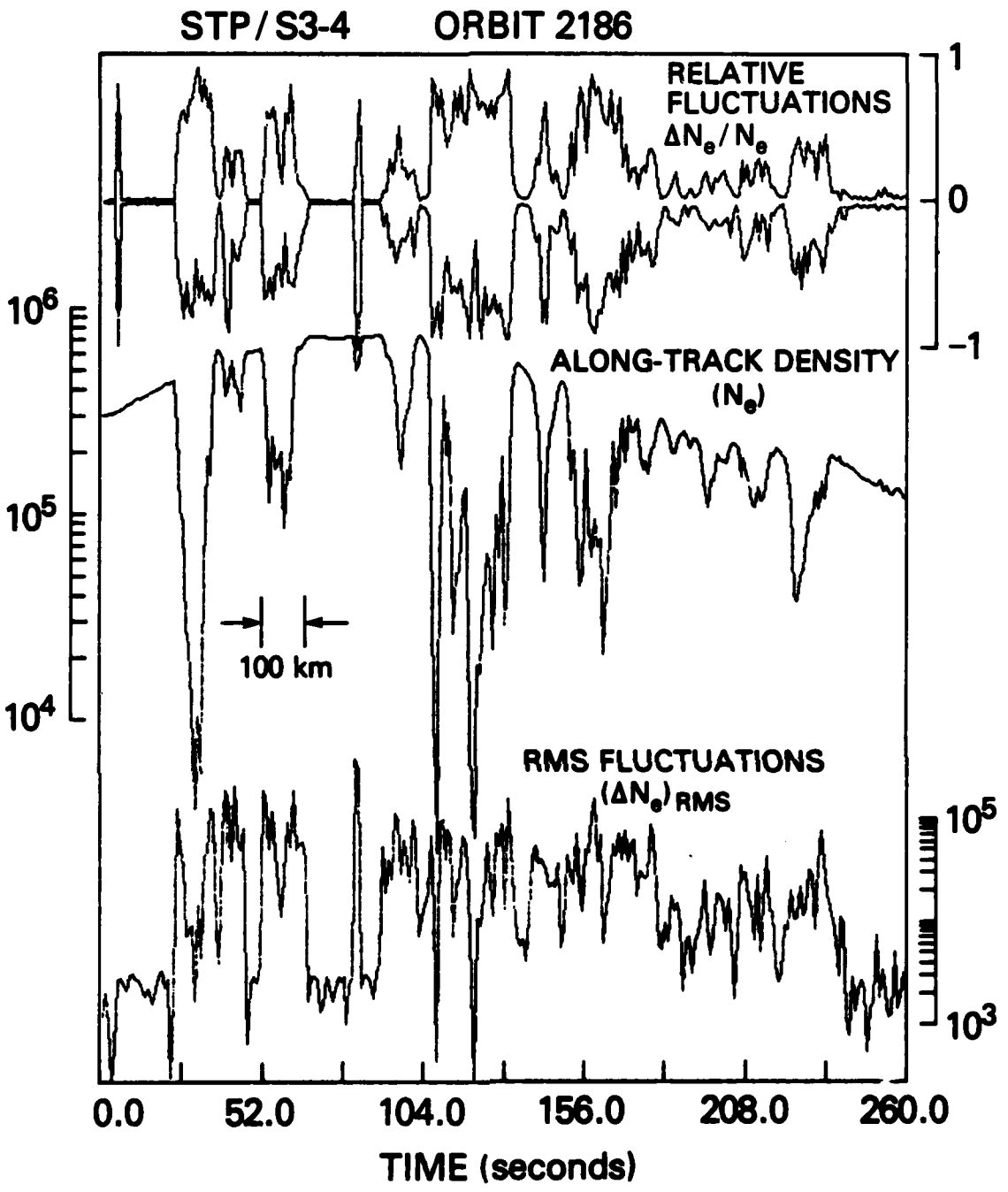

UT	9:28:00	9:32:20
LT	22:28:39	22:20:34
LAT	20.9°S	3.7°S
LONG	196.7°E	193.6°E

Figure 4. S3-4 measurements of nighttime equatorial plasma irregularities. The middle panel displays the absolute in-track ionospheric density profile. The upper and lower panels are the associated percent fluctuations $\Delta N_e/N_e$, and RMS variations ΔN_e(RMS) respectively.

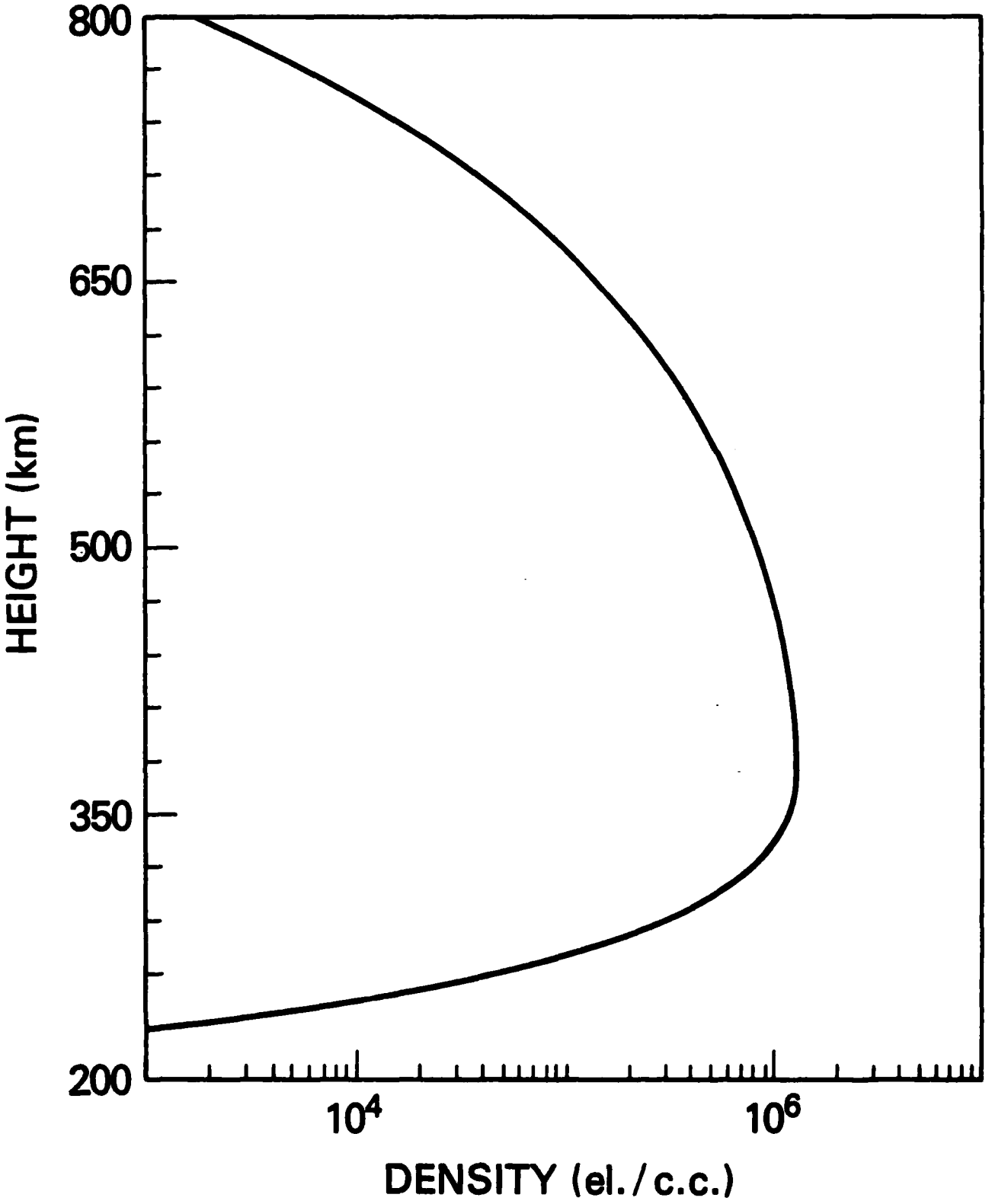

Figure 5. Chapman profile used in phase path calculations with superimposed irregularity distributions.

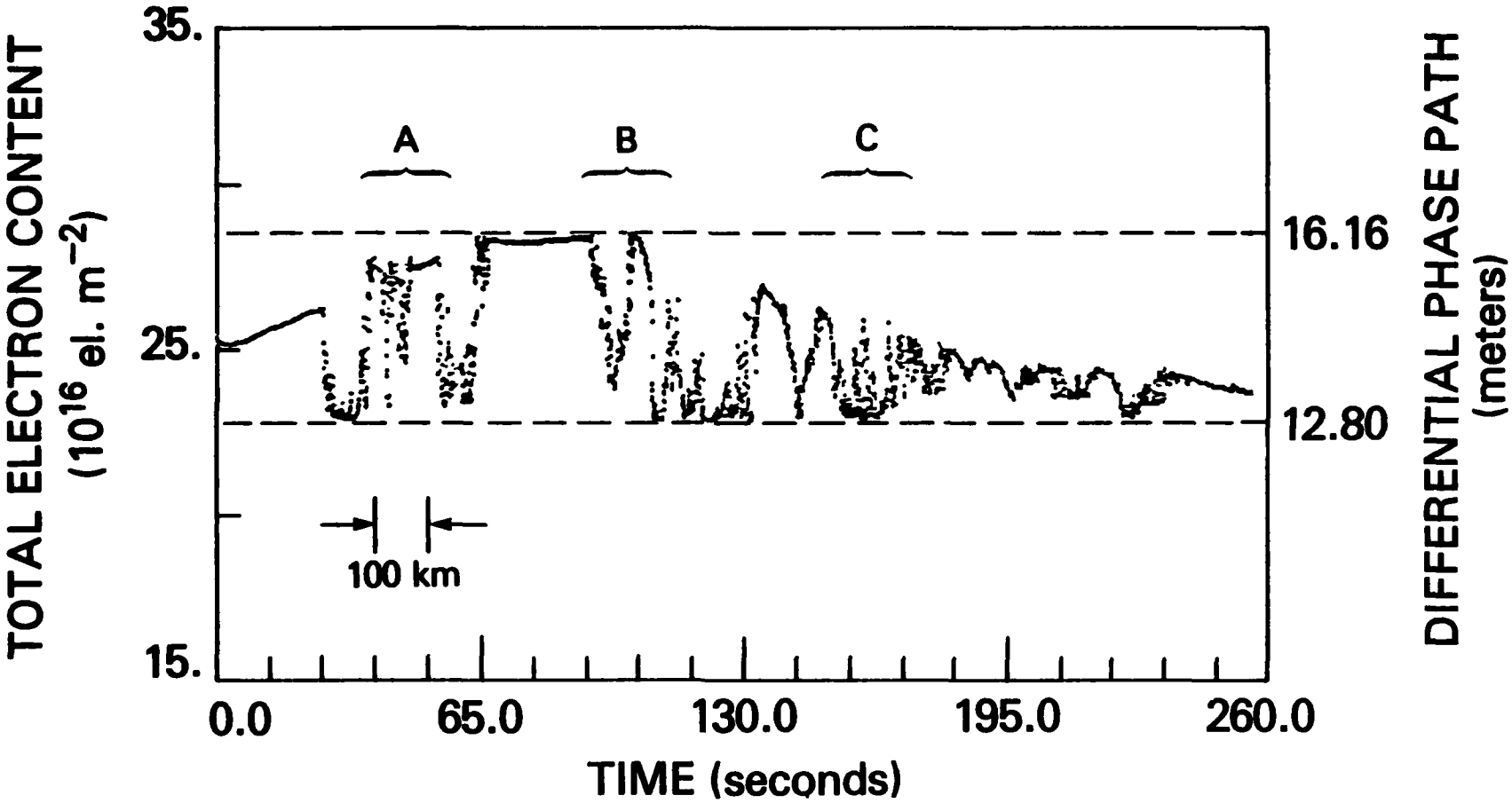

Figure 6. Total electron content (left-hand ordinate) and two-way phase path (right-hand ordinate) fluctuations associated with the ionospheric irregularity distribution shown in Figure 4 and the Chapman profile in Figure 5.

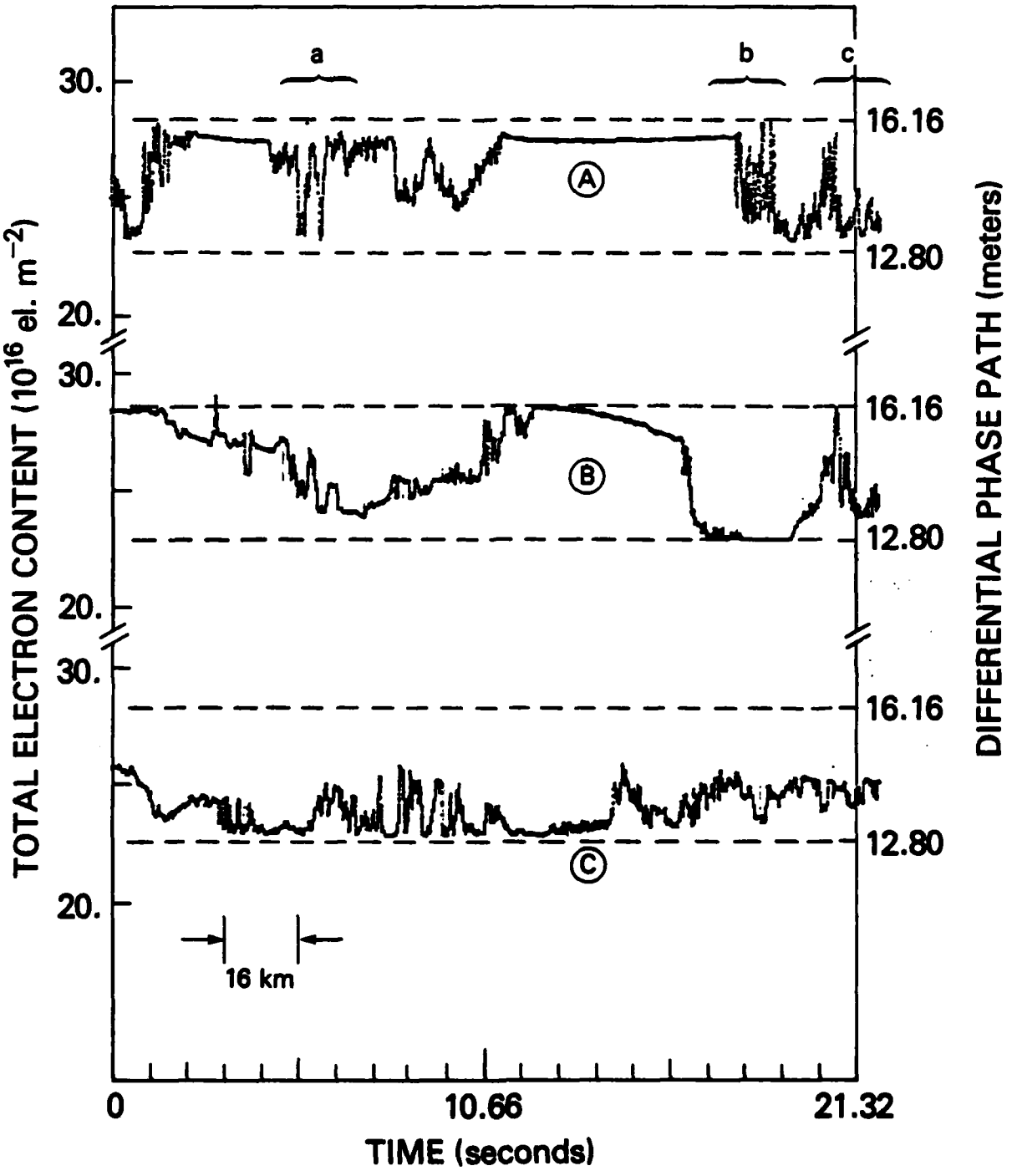

Figure 7. Expanded 160 kilometer segments (approximately 10 synthetic aperture lengths) from Figure 6.

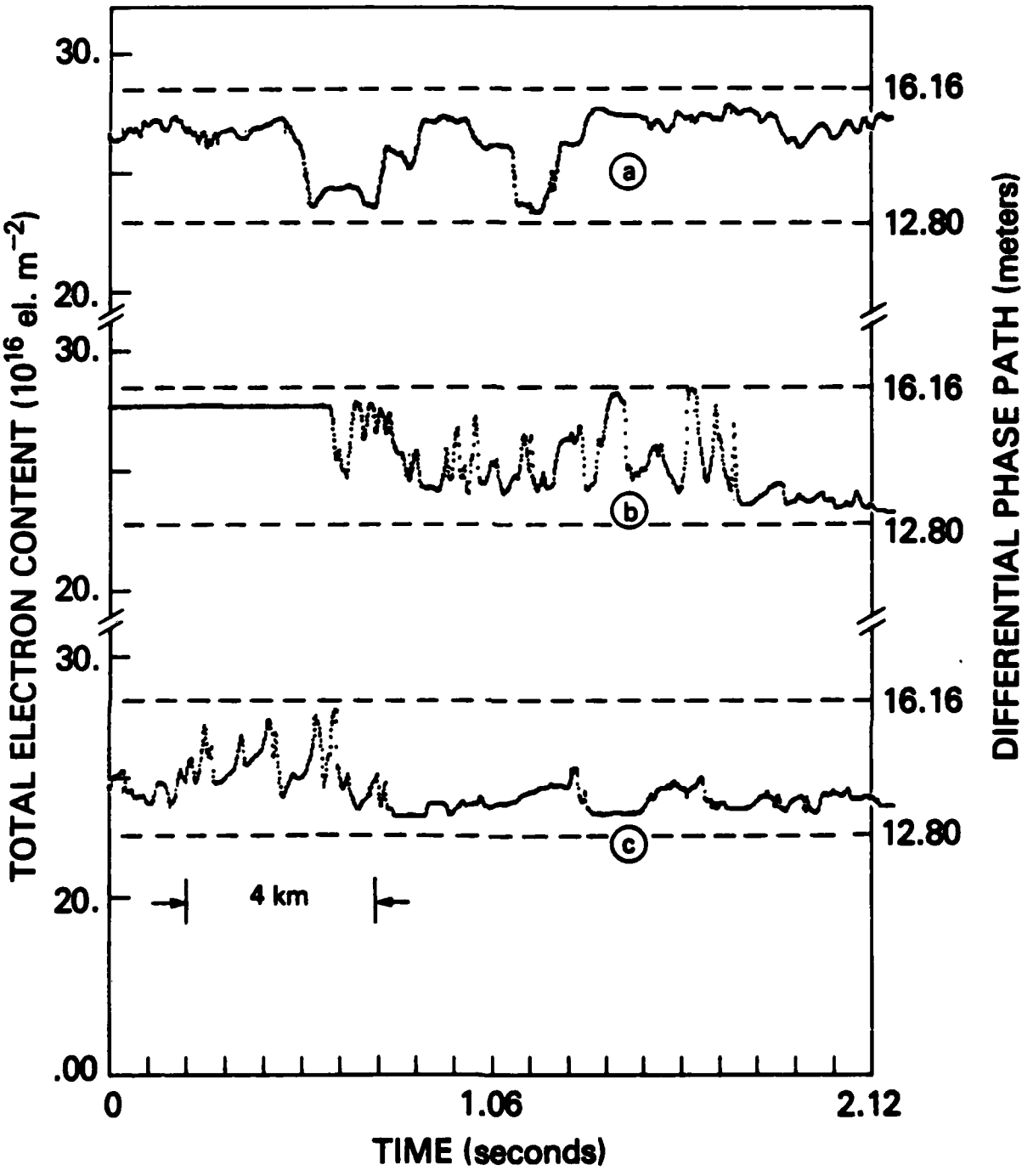

Figure 8. Expanded 16 kilometer segments (approximately 1 synthetic aperture length) from Figure 7.

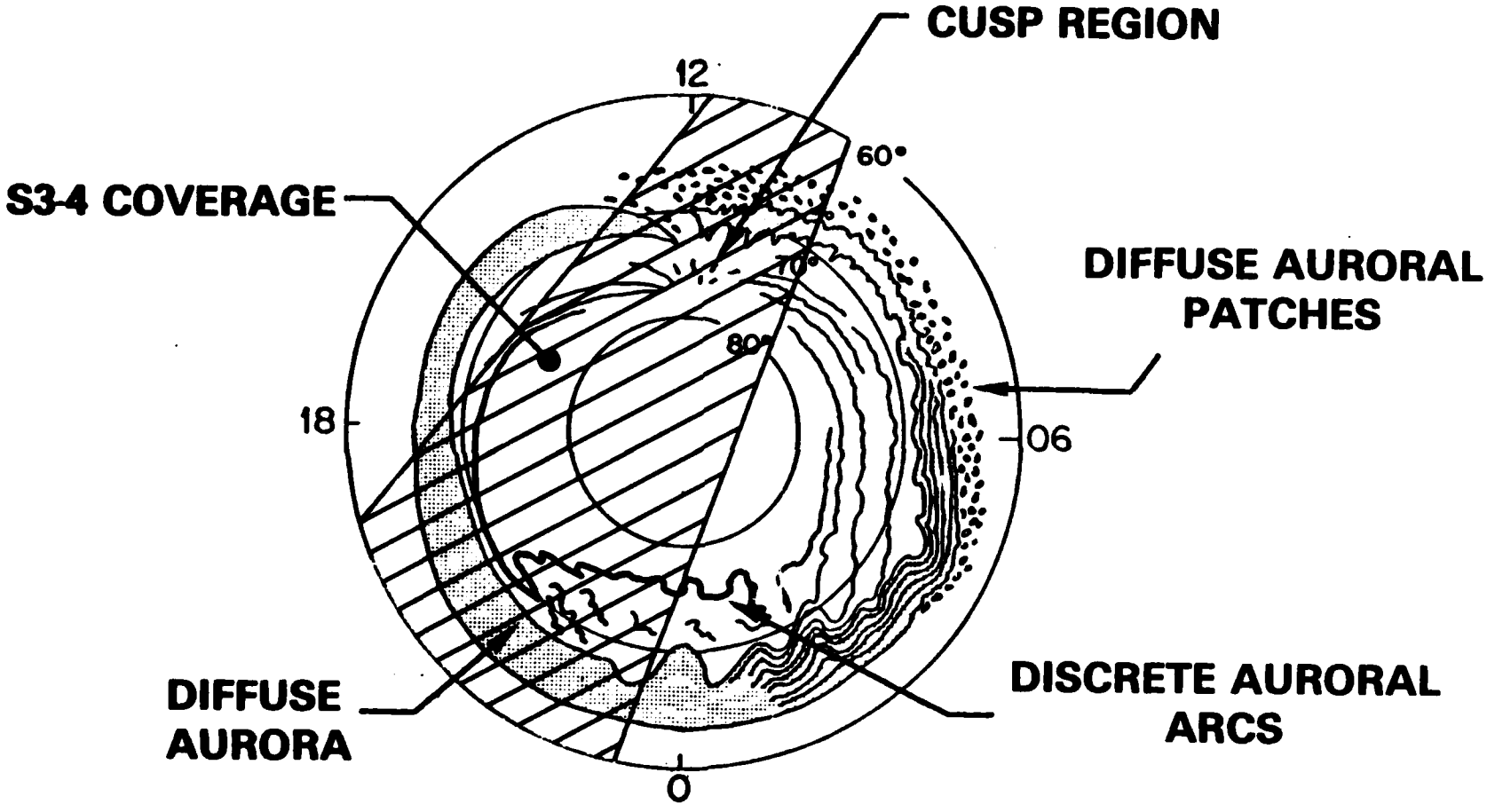

Figure 9. A phenomenological source-term map of high-latitude ionospheric irregularities showing regions covered by the S3-4 satellite. (Adapted from S.I. Akosofu, Sp. Science Rev. 19, 169 (1976)). The diagram shows major phenomenological elements in dipole-MLT coordinates.

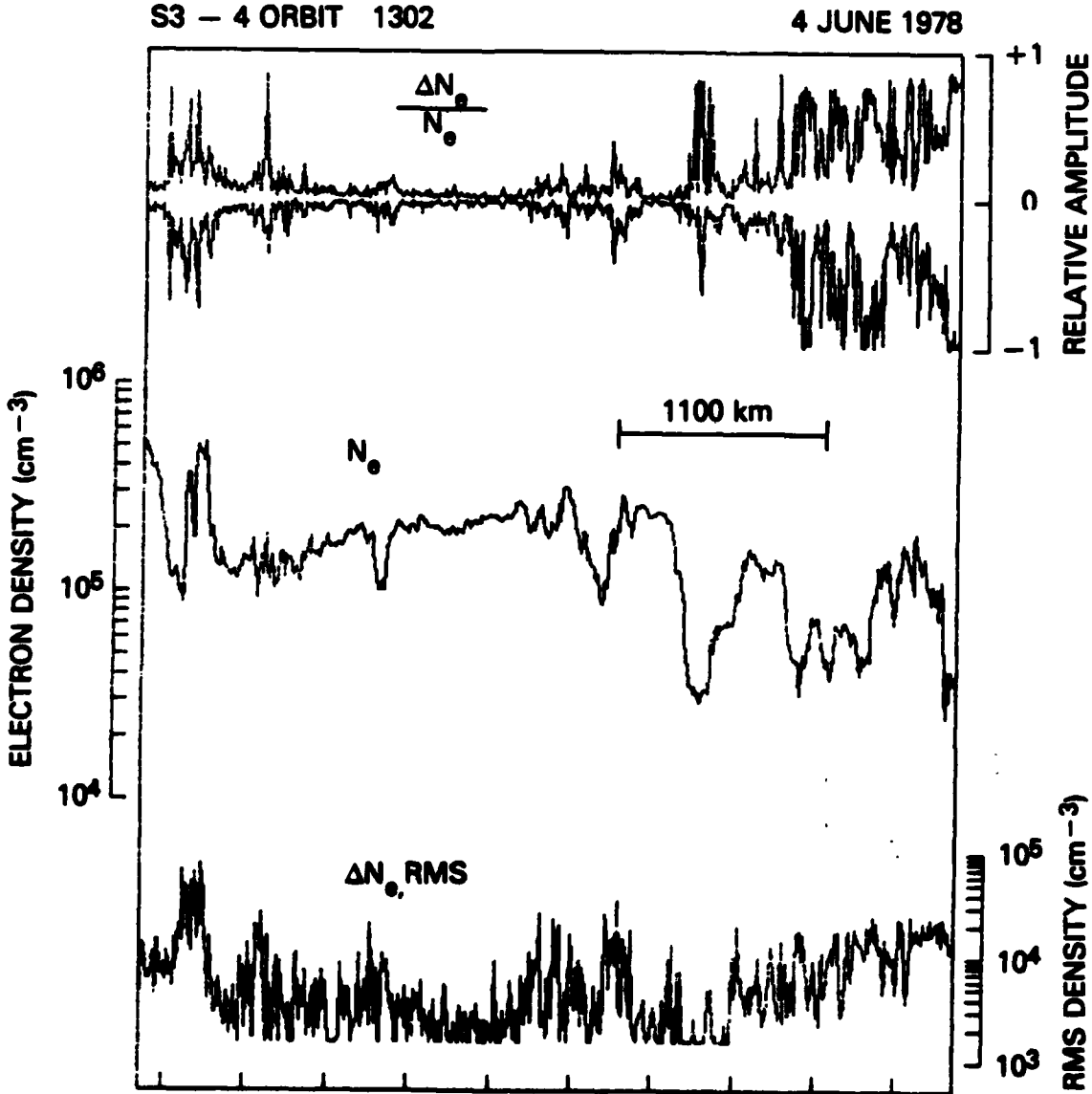

UT	2204	2206	2208	2210	2212	(HRMN)
GLAT	–61.3	–69.1	–76.5	–82.5	–82.5	(°)
GLON	173.7	168.0	156.8	125.9	61.0	(°)
MLAT	–64.3	–72.2	–79.8	–85.3	–81.5	(°)
MLT	1127	1147	1239	1618	2042	(HRMN)
ALT	255.0	263.4	270.3	275.8	280.1	(KM)

Figure 10. S3-4 measurements of ionospheric irregularities in the polar cap. The middle panel displays the absolute in-track ionospheric density profile. The upper and lower panels are the associated percent fluctuations $\Delta N_e/N_e$, and RMS variations ΔN_e(RMS) respectively.

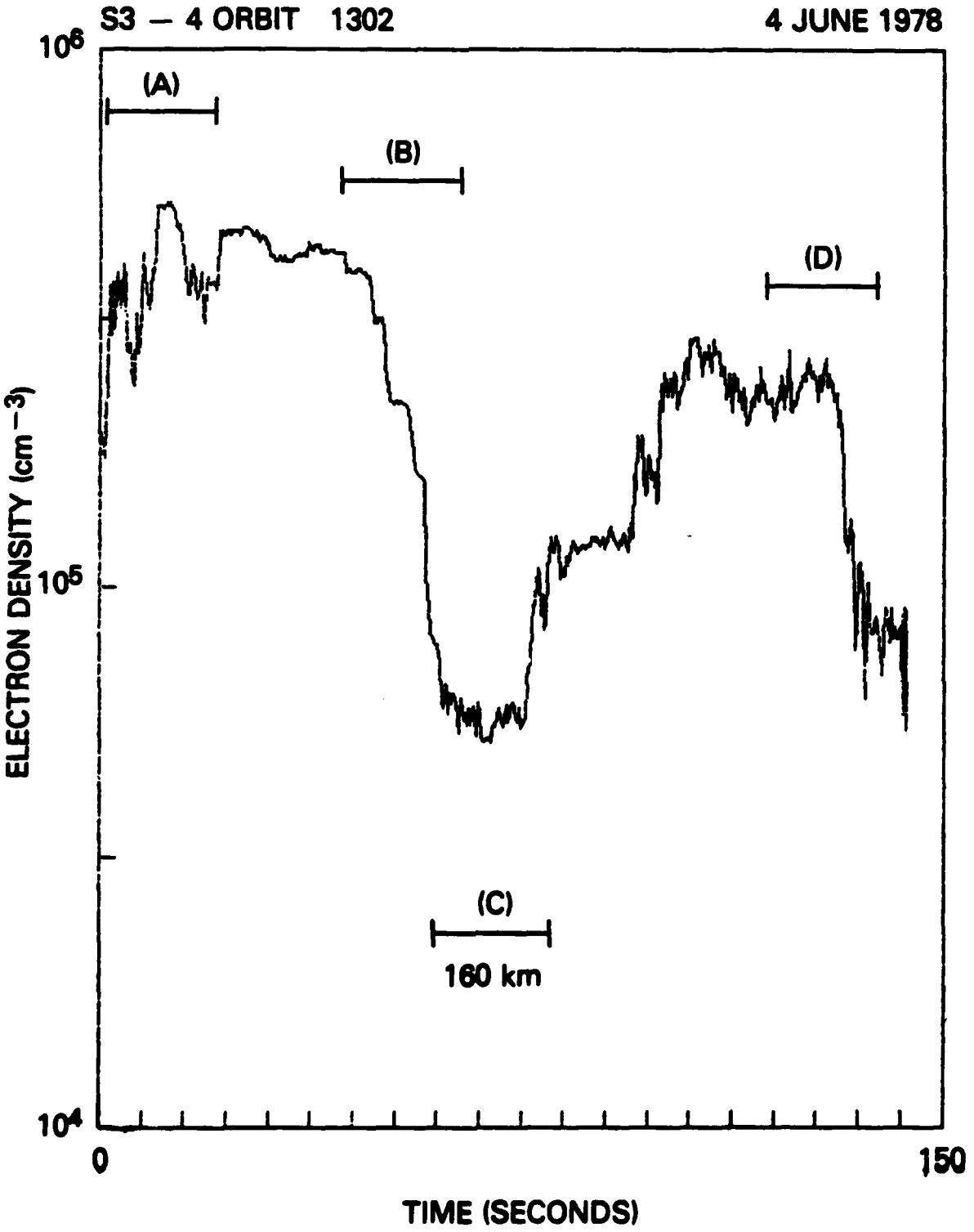

Figure 11. An expanded view of an 1100 km segment of the data in Figure 10.

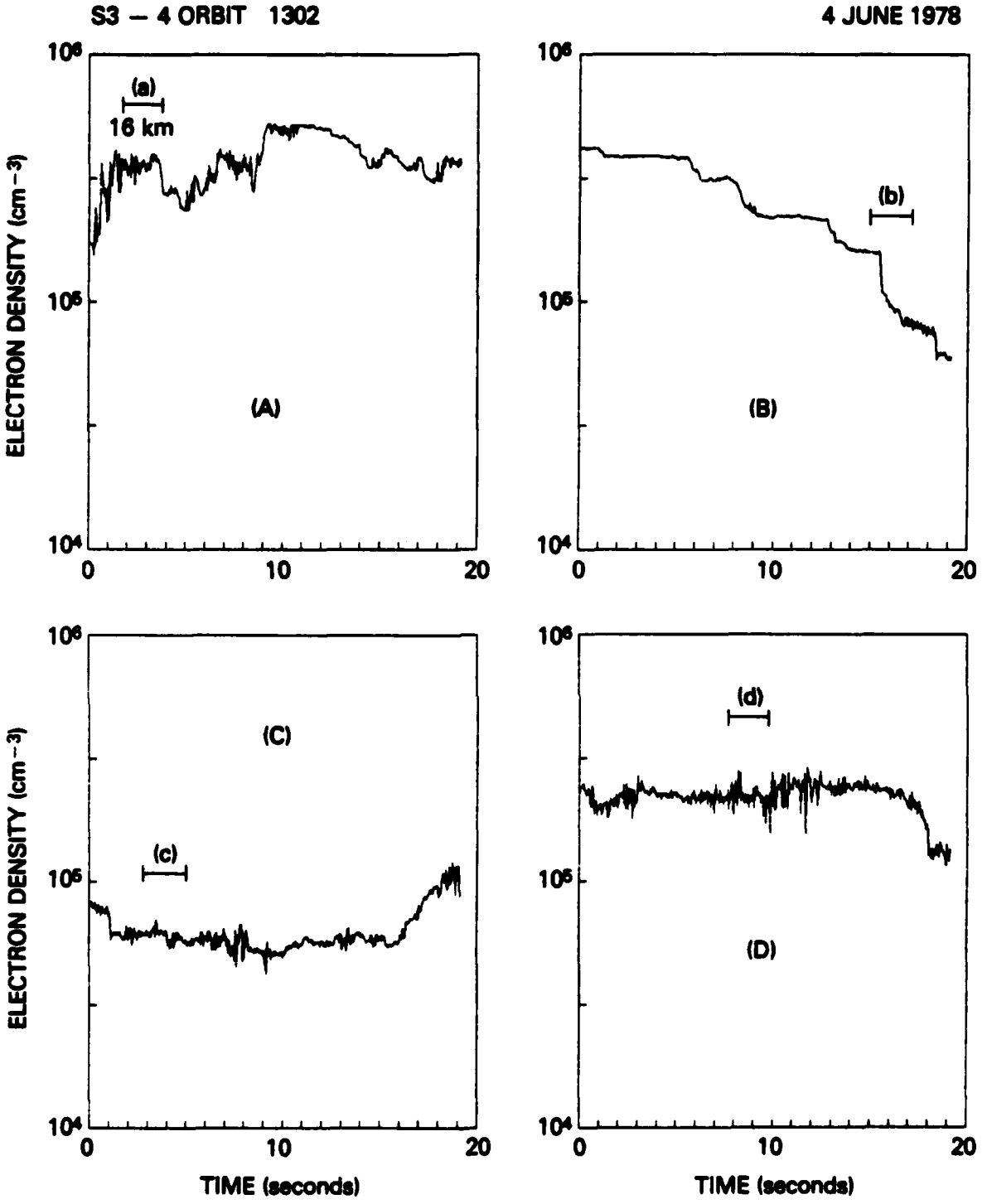

Figure 12. Expanded 160 km segments (approximately 10 synthetic aperture lengths) of plasma irregularities from Figure 11.

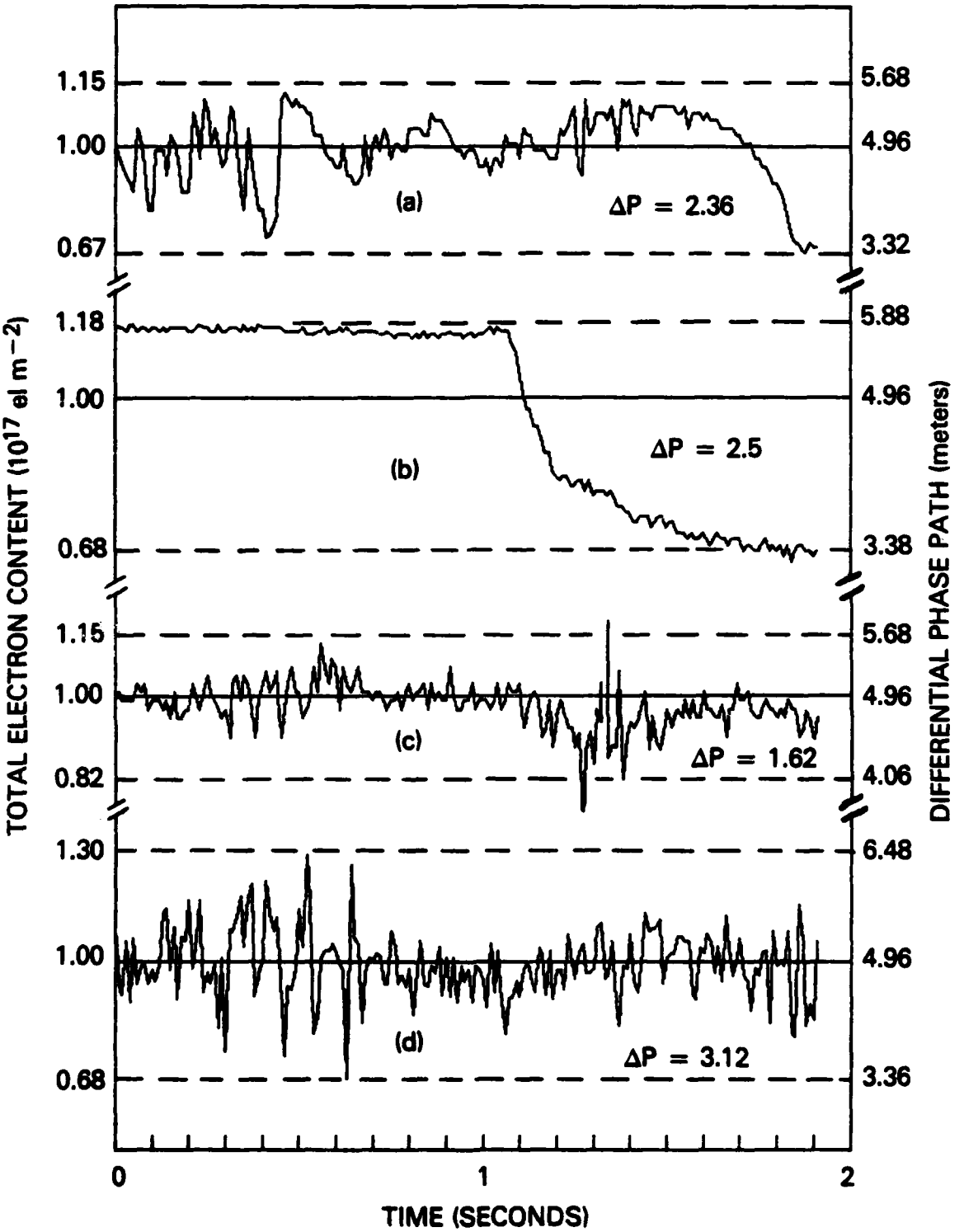

Figure 13. Expanded 16 km segments of phase path fluctuations associated with portions of the plasma irregularities in Figure 12. (16 km is approximately one aperture length for the Seasat SAR.) The inserted values for ΔP represent the phase path variation between the dashed lines.

ACKNOWLEDGEMENT

The authors wish to thank the Naval Electronic System Command and the Office of Naval Research for support throughout this program. This work was supported by the Naval Electronics System Command under program element #62712N and project #XF12-141-350. The work was also supported within the Ionospheric and Stratospheric Task Area (41-0949) and conducted within the Space Plasma Diagnostics Group of the Naval Research Laboratory's Space Science Division.

REFERENCES

Fremouw, E. J., C. L. Rino, R. C. Livingston, and M. C. Cousins (1977), A persistent subauroral scintillation enhancement observed in Alaska, Geophys. Res. Lett. 4, 539.

Harger, R. O. (1970), Synthetic aperture radar systems: theory and design, Academic Press, New York, New York.

Kelley, M. C., R. Pfaff, K. D. Baker, J. C. Ulwick, R. Livingston, C. Rino, and R. Tsunoda (1982), Simultaneous rocket probe and radar measurements of equatorial spread-F transitional and short wavelength results, J. Geophys. Res. 87, 1575.

Keskinen, M. J., E. P. Szuszczewicz, S. L. Ossakow, and J. C. Holmes (1981), Nonlinear theory and experimental observations of the local collisional Rayleigh-Taylor instability in a descending equatorial spread-F ionosphere, J. Geophys. Res. 86, 5785.

McClure, J. P., and W. B. Hanson (1973), A catalog of ionospheric F-region irregularity behavior based on Ogo-6 retarding potential analyzer update, J. Geophys. Res. 78, 7431.

McClure, J. P., W. B. Hanson, and J. H. Hoffman (1977), Plasma bubbles and irregularities in the equatorial ionosphere, J. Geophys. Res. 82, 2650.

Narcisi, R. S., and E. P. Szuszczewicz (1981), Direct measurements of electron density, temperature and ion composition in an equatorial spread-F ionosphere, J. Atm. Terr. Phys. 43, 463.

Rino, C. L., R. C. Livingston, and S. J. Matthews (1978), Evidence for sheet-like auroral ionospheric irregularities, Geophys. Res. Lett. 5, 1039.

Rodriguez, P., M. Singh, E. P. Szuszczewicz, D. N. Walker, and J. C. Holmes (1981), The STP/S3-4 satellite experiment: High latitude large scale density irregularities, Proceedings 1981 Symposium on the Effect of the Ionosphere on Radio Wave Systems (1981, in press), J. M. Goodman, editor, U.S. Government Printing Office, Wash., DC; NRL Memorandum Report #4514.

Szuszczewicz, E. P., J. C. Holmes, and M. Singh (1982a), The S3-4 ionospheric irregularities satellite experiment: Probe detection of multi-ion component plasmas and associated effects on instability processes, Astrophysics and Space Science 86, 235 (1982).

Szuszczewicz, E. P., J. C. Holmes, D. N. Walker, P. Rodriguez, M. Swinney, L. Kegley, and M. Singh (1982), An atlas of Ionospheric F-region structures as determined by the NRL-747/S3-4 ionospheric irregularities satellite investigation, NRL Memo Report #4862.

Szuszczewicz, E. P.(1977), Ionospheric holes and equatorial spread-F; chemistry and transport, J. Geophys. Res. 82, 5073.

Szuszczewicz, E. P., M. Singh, and J.C. Holmes (1981), Satellite and rocket observations of equatorial spread-F irregularities: A two-dimensional model, J. Atm. Terr. Phys., 43, 779

Szuszczewicz, E. P., R. T. Tsunoda, R. Narcisi, and J. C. Holmes (1980), Coincident radar and rocket observations of equatorial spread-F, Geophys. Res. Lett. 7, 537.

Tomiyasu, K. (1978), Tutorial review of synthetic-aperture radar (SAR) with applications to imaging of the ocean surface, Proc. IEEE 66, 563.

Wu, C. (1980), A digital fast correlation approach to produce Seasat SAR imagery, in proceedings IEEE International Radar Conference, IEEE Aerospace and Electronic System Society, Arlington, VA, pp. 153-160.

END

FILMED

3-83

DTIC